Supporting Information

Molecularly Engineered Li Compensation Agent-Integrated Separator Enabling Regeneration of Degraded $LiFePO_4$

Fujun Tao, [†a] Zeyi Yao, [†a] Jiahui Hou,[a] Zexin Wang,[a] Zhenzhen Yang,[b] and Yan Wang*[a]

[a]Department of Material Science and Engineering, Worcester Polytechnic Institute, 100 Institute Rd, Worcester, MA 01609, USA

[b]Chemical Sciences and Engineering Division, Argonne National Laboratory, 9700 S Cass Ave, Lemont, IL 60439, USA

[†]These authors contribute equally to this work.

* Corresponding author.

E-mail: yanwang@wpi.edu

The PDF file includes:

1. Supporting Figures

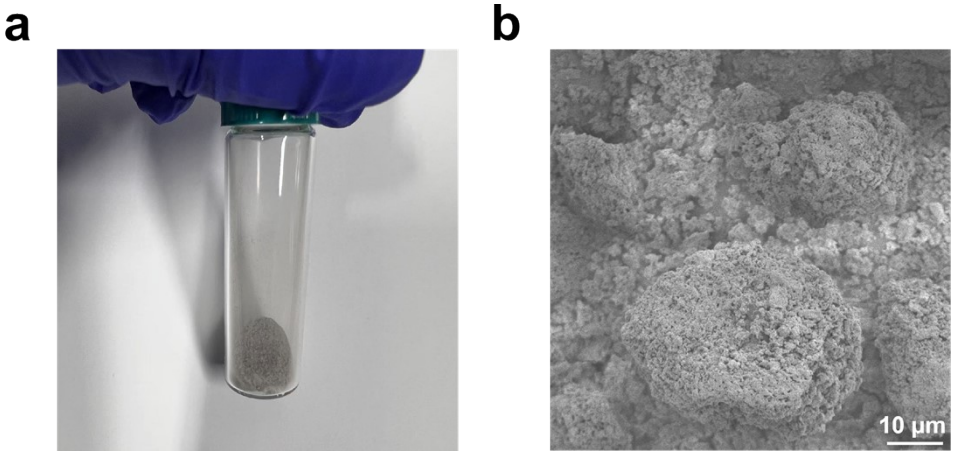

Fig. S1 (a) Photo and (b) SEM image of the as-synthesized LTFBB.

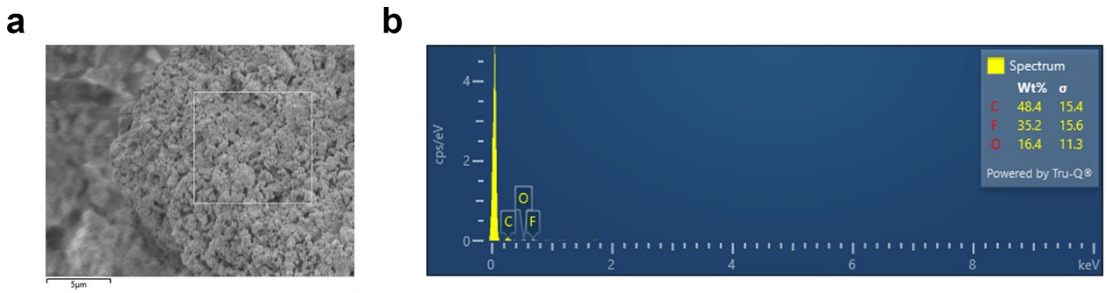

Fig. S2 EDS spectrum of as-synthesized LTFBB.

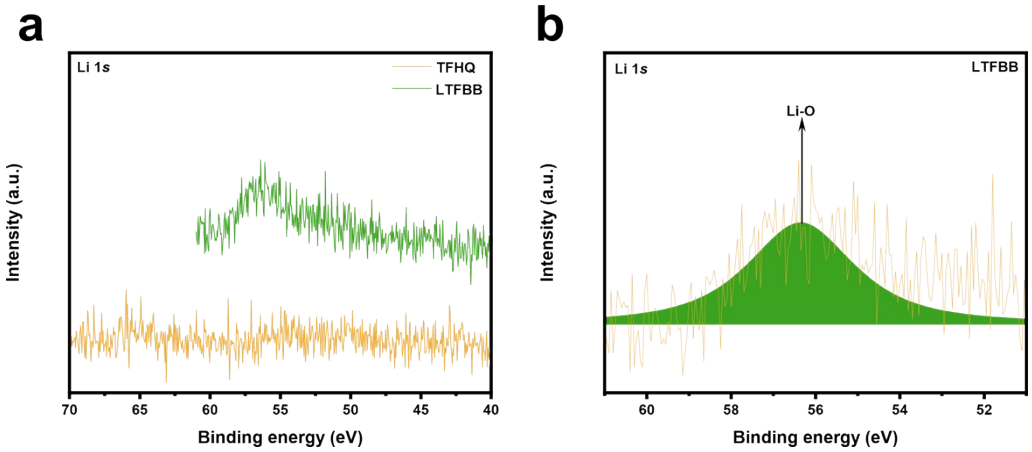

Fig. S3 (a) Li 1s XPS spectra of TFHQ and LTFBB. (b) Li 1s XPS spectrum of LTFBB with fitted curves.

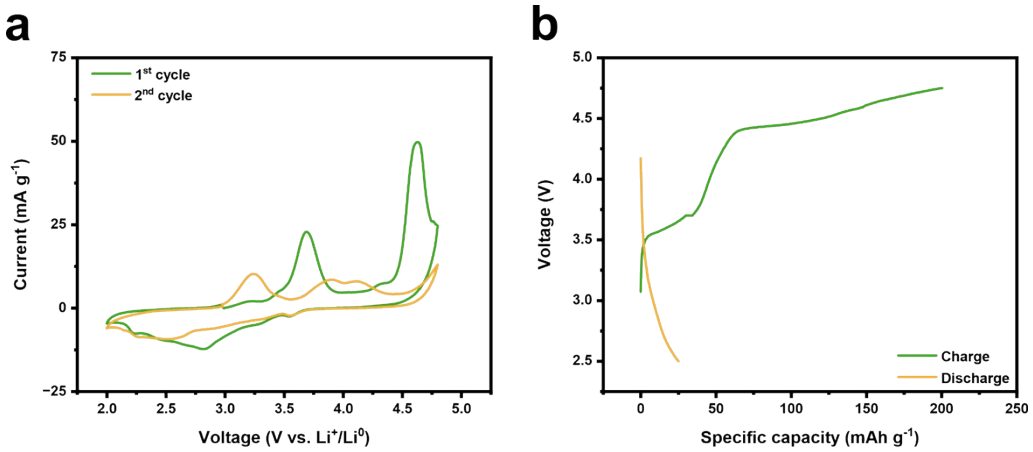

Fig. S4 (a) CV curves and (b) galvanostatic charge-discharge profiles of the LTFBB electrode with Super C65 as the conductive carbon.

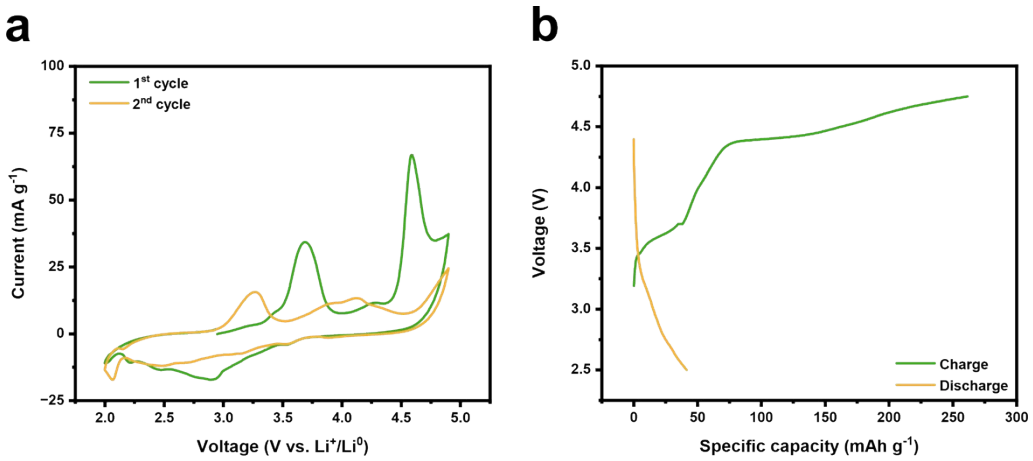

Fig. S5 (a) CV curves and (b) galvanostatic charge-discharge profiles of the LTFBB electrode with Super C65&CMK as the conductive carbon.

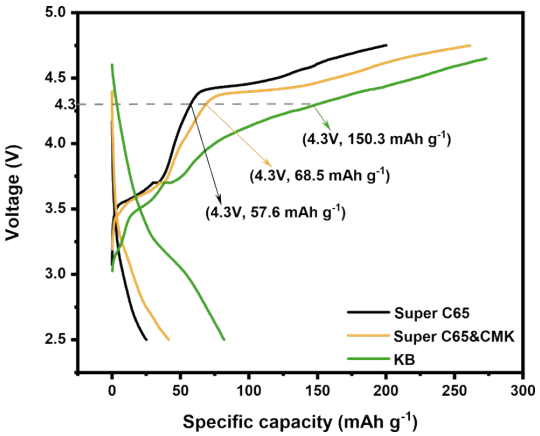

Fig. S6 Galvanostatic charge-discharge profiles of the LTFBB electrode with Super C65, Super C65&CMK, and KB as the conductive carbon, respectively.

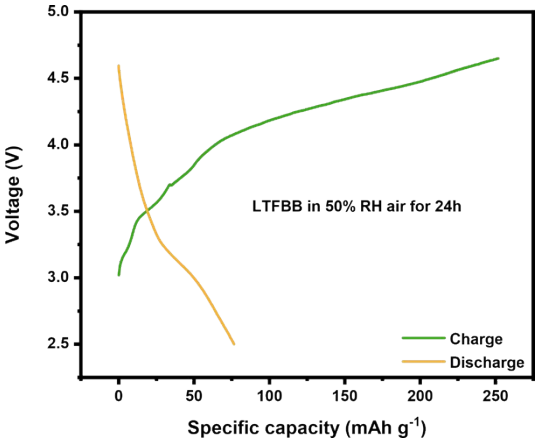

Fig. S7 Galvanostatic charge-discharge profiles of the LTFBB after it being exposed to 50% RH air for 24 hours, respectively.

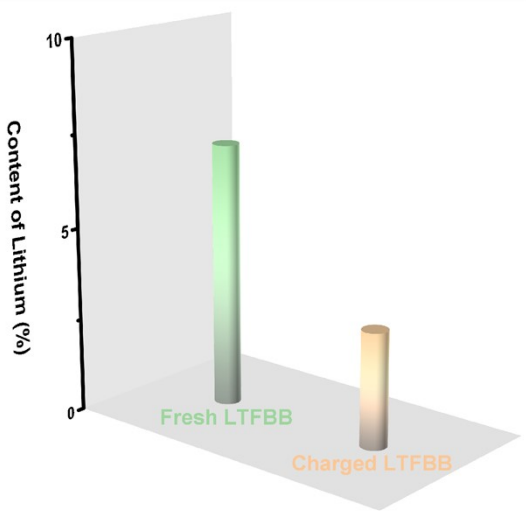

Fig. S8 Lithium content of fresh LTFBB and of LTFBB after charging to 4.3 V, respectively.

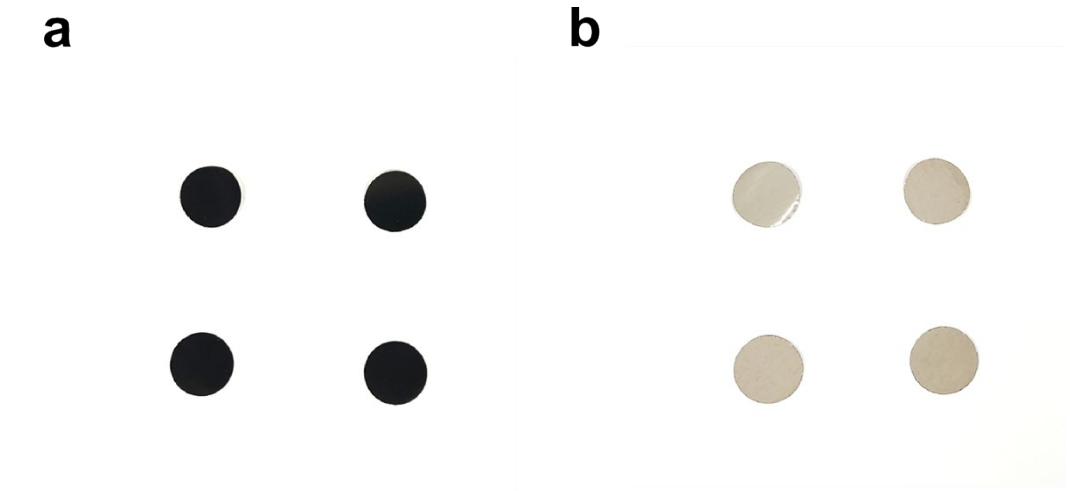

Fig. S9 Photos of (a) the coated side and (b) the back side of LRS.

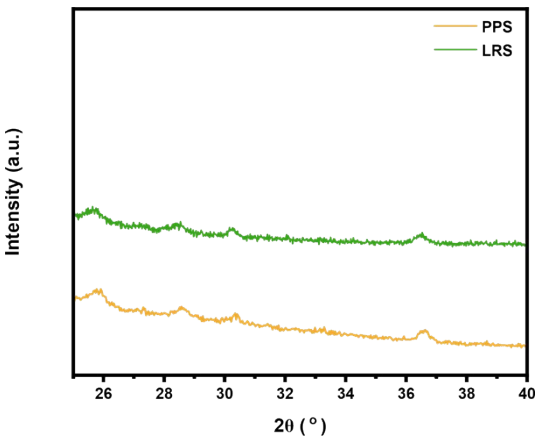

Fig. S10 XRD patterns of PPS and LRS over the region from 25° to 40°.

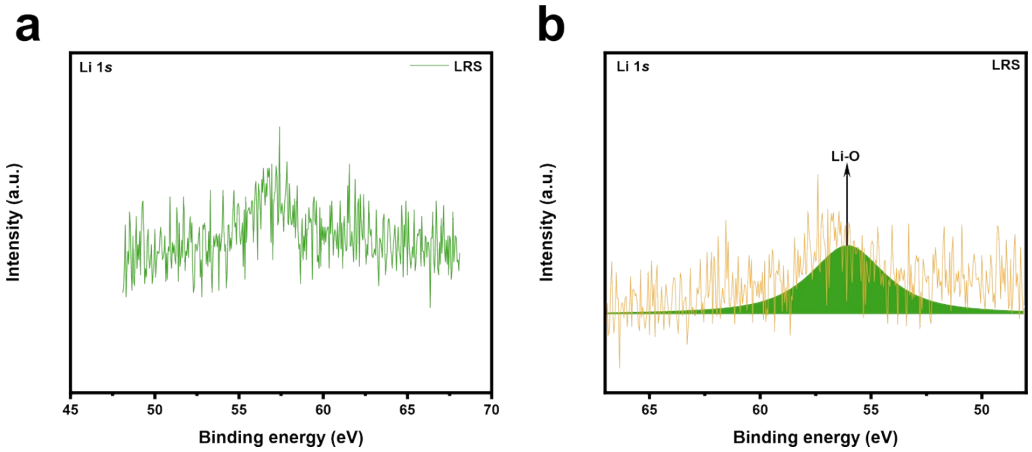

Fig. S11 (a) Li 1s XPS spectrum of LRS and (b) corresponding fitted curves.

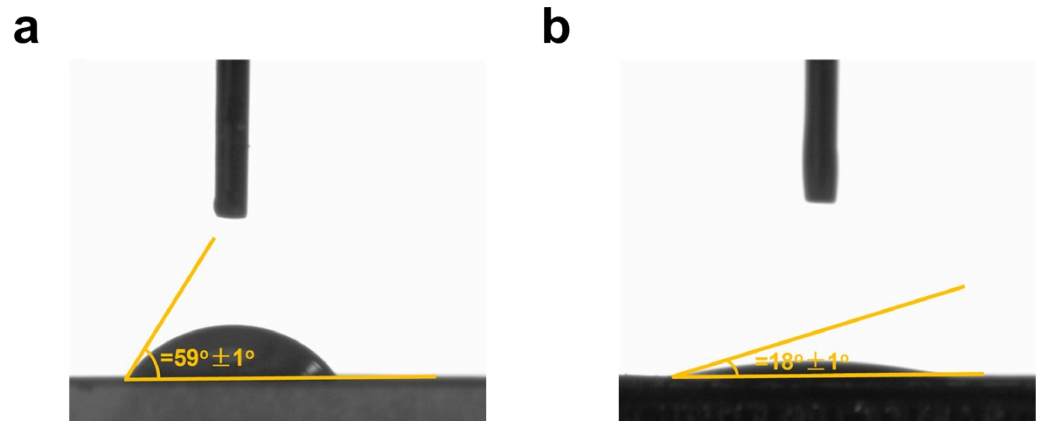

Fig. S12 Contact angles of (a) PPS and (b) LRS.

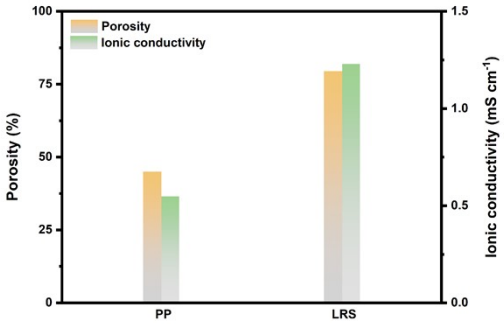

Fig. S13 The porosity and ionic conductivity of (a) PPS and (b) LRS.

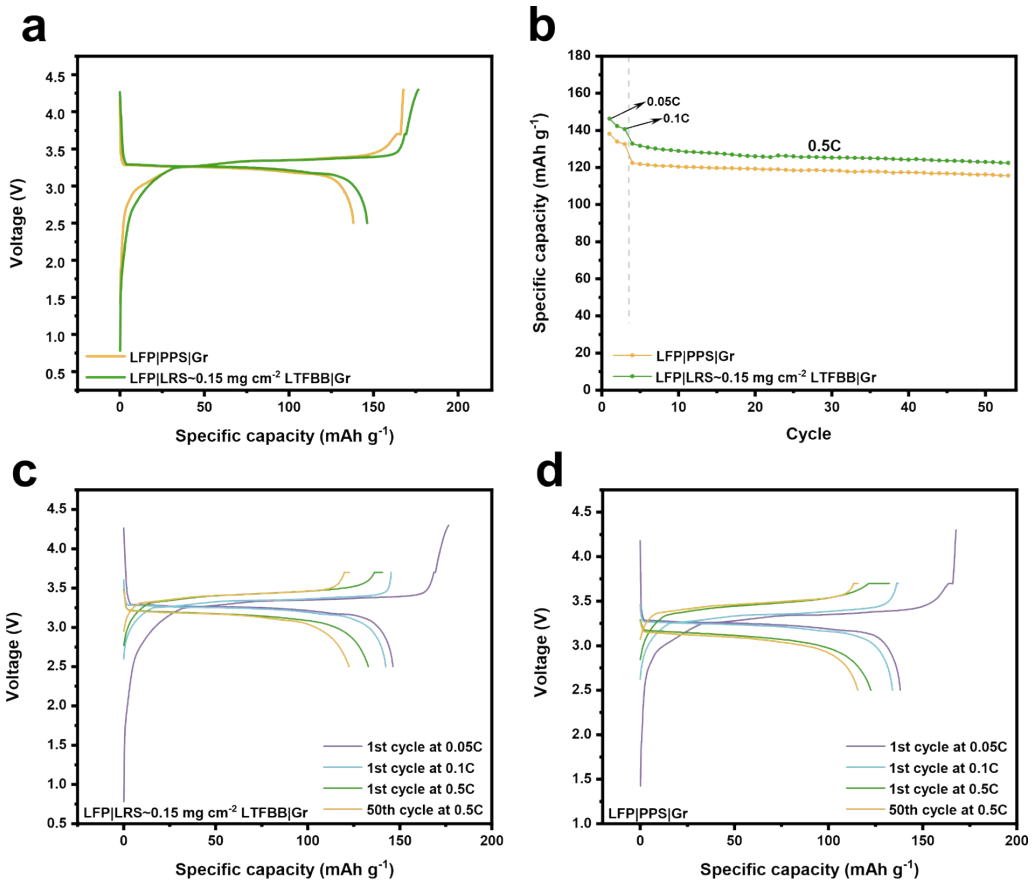

Fig. S14 Electrochemical performance of LFP||Gr full cells with LRS~0.15 mg cm^{-2} LTFBB and PPS. (a) Initial charge-discharge profiles at 0.05C. (b) Cycling performance. Charge-discharge profiles of the full cells with (c) LRS and (d) PPS at various cycles numbers.

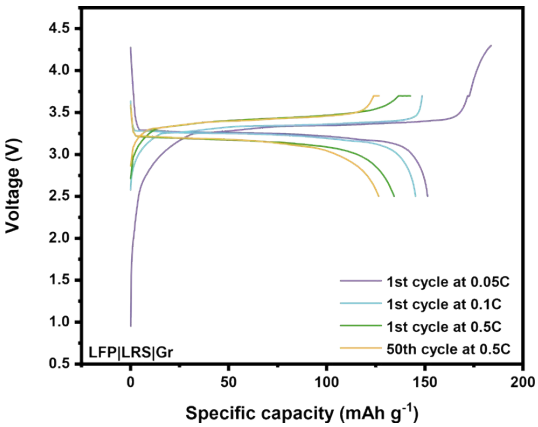

Fig. S15 Charge-discharge profiles of the full cells with LRS~0.3 mg cm^{-2} LTFBB at various cycles numbers.

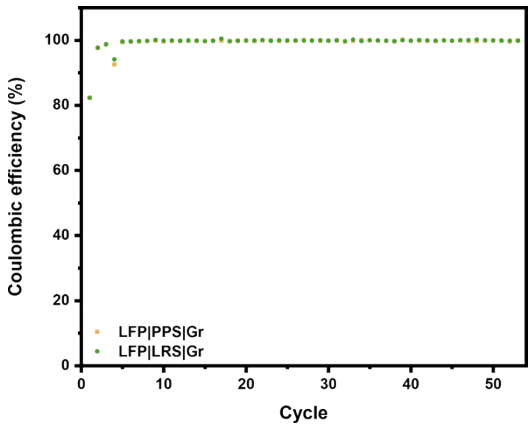

Fig. S16 Coulombic efficiency of LFP‖Gr full cells equipped with LRS and PPS.

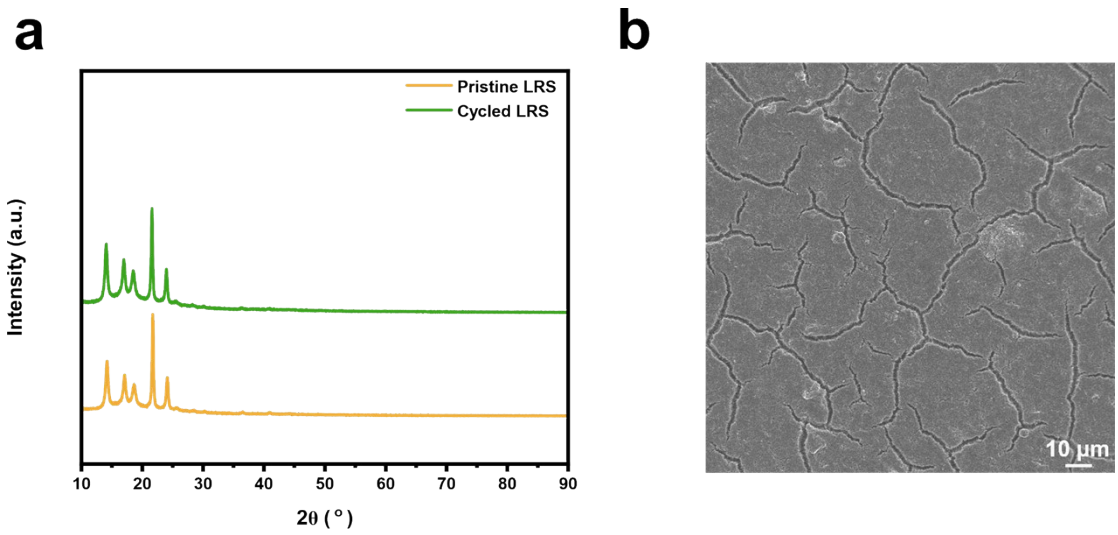

Fig. S17 XRD patterns of the pristine and cycled LRS, and SEM image of the LRS after cycling.

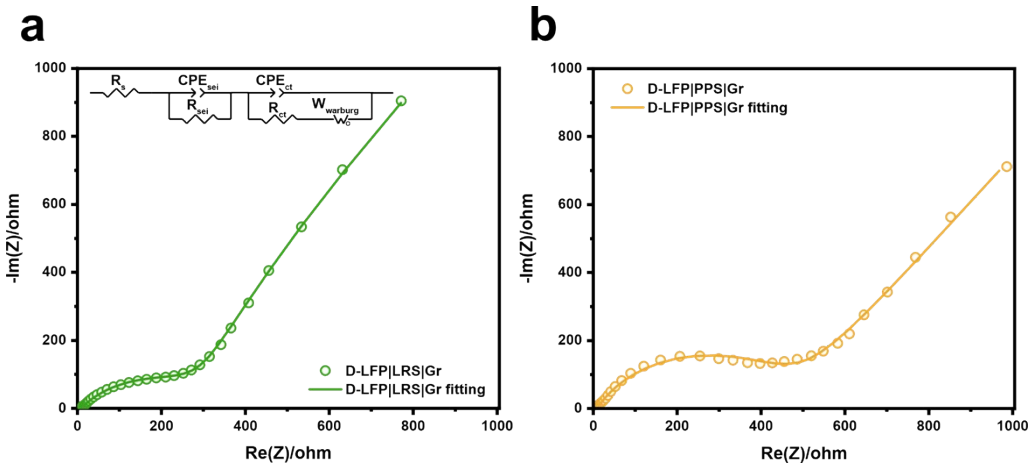

Fig. S18 Raw and fitted Nyquist plots of the impedance spectra for D-LFP||Gr full cells with (a) LRS or (b) PPS after formation.

As shown in Figure S18, the fitting data show that the LRS cell (Figure S18a) exhibits a lower R_s of 8.2 Ω and an R_{sei} of 323 Ω with a $\chi^2/|Z|$ of 0.025, compared to the PPS cell (Figure S18b), which has an R_s of 8.9 Ω and an R_{sei} of 455.7 Ω with a $\chi^2/|Z|$ of 0.051.

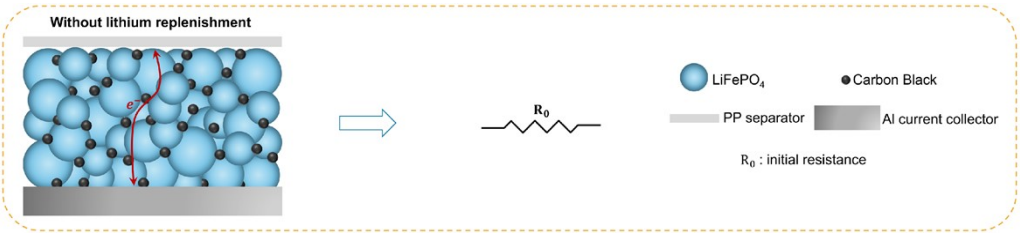

Fig. S19 Effect of PPS on resistance.

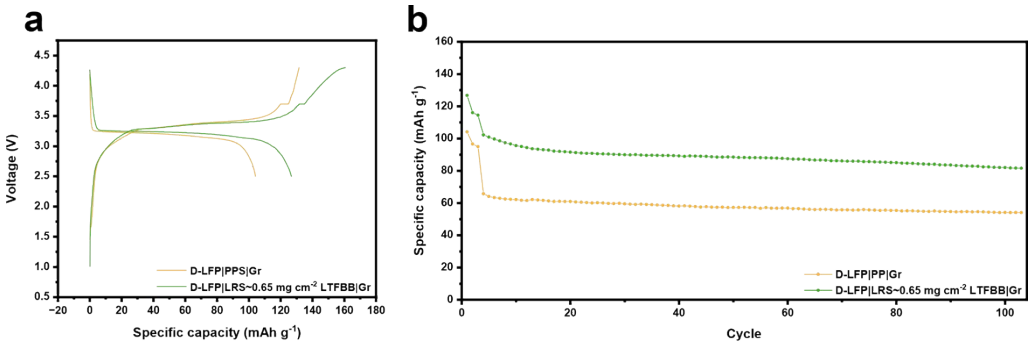

Fig. S20 Electrochemical performance of D-LFP||Gr full cells with LRS~0.65 mg cm^{-2} LTFBB and PPS. (a) Initial charge-discharge profiles at 0.05C. (b) Cycling performance.

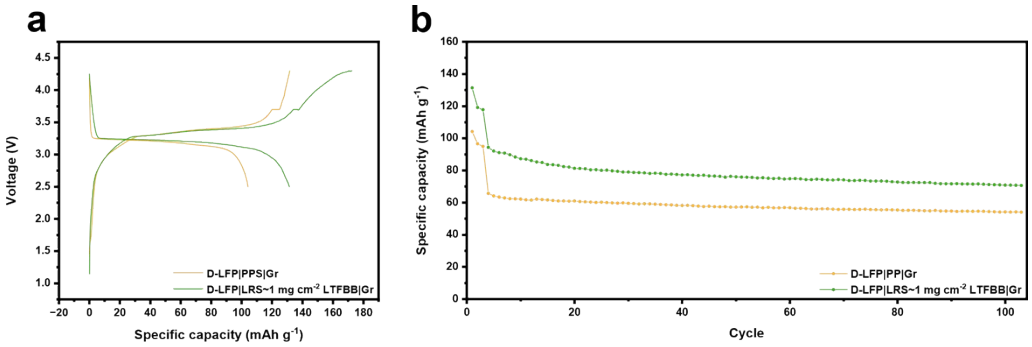

Fig. S21 Electrochemical performance of D-LFP||Gr full cells with LRS~1 mg cm^{-2} LTFBB and PPS. (a) Initial charge-discharge profiles at 0.05C. (b) Cycling performance.

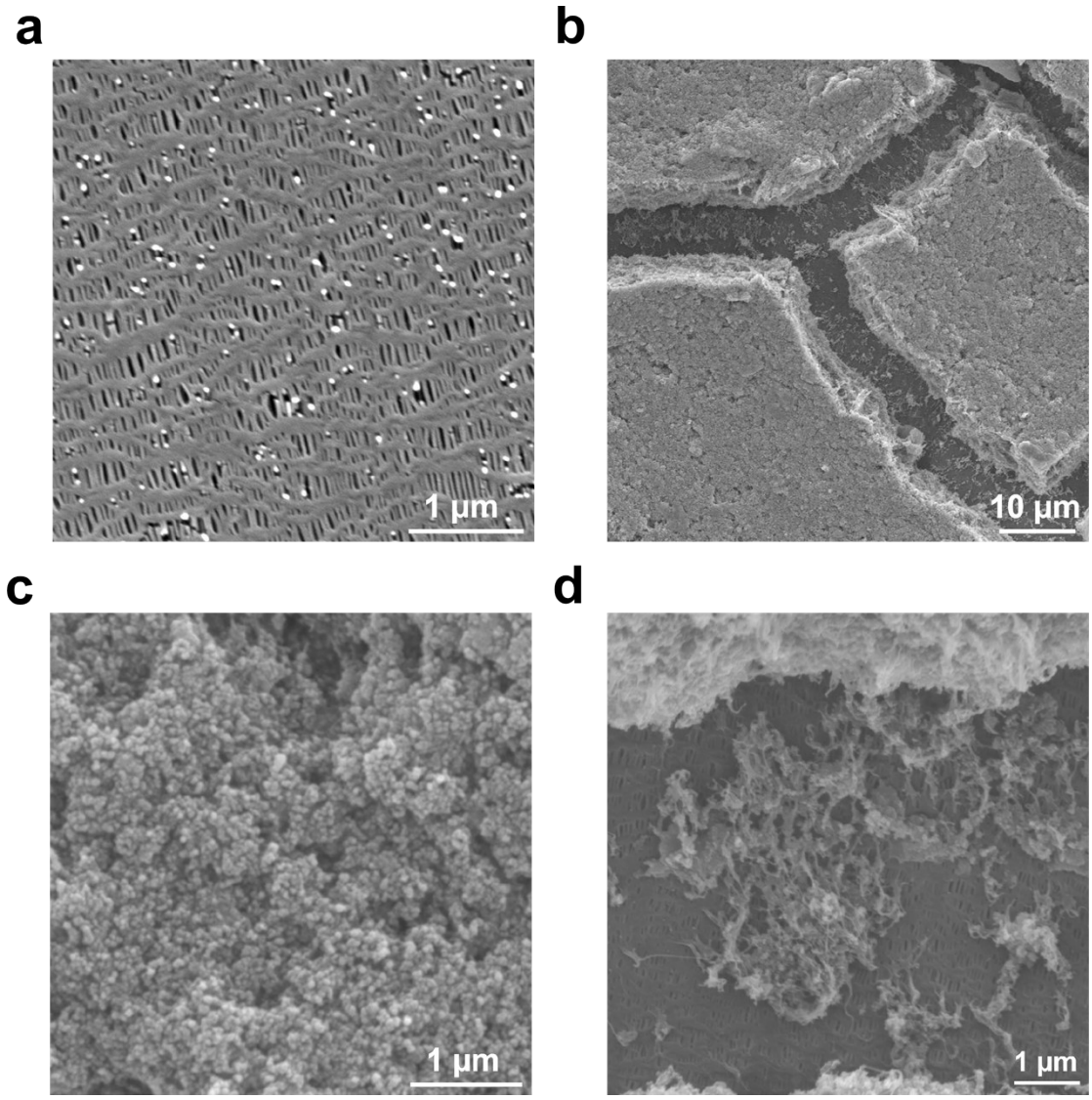

Fig. S22 SEM images of the (a) PPS, (b) LRS~1 mg cm^{-2} LTFBB, (c) main part of the coating on the LRS, and (d) the cracked region of the coating on the LRS.

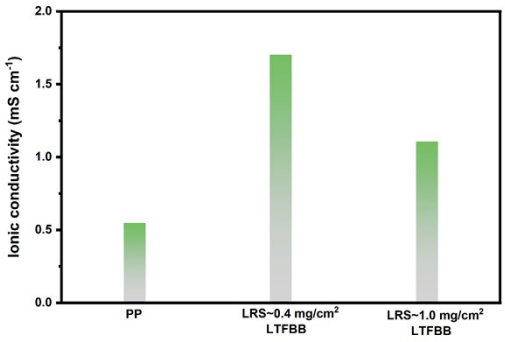

Fig. S23 The ionic conductivity of PPS, LRS~0.4 mg/cm^2 LTFBB, and LRS~1.0 mg/cm^2 LTFBB.

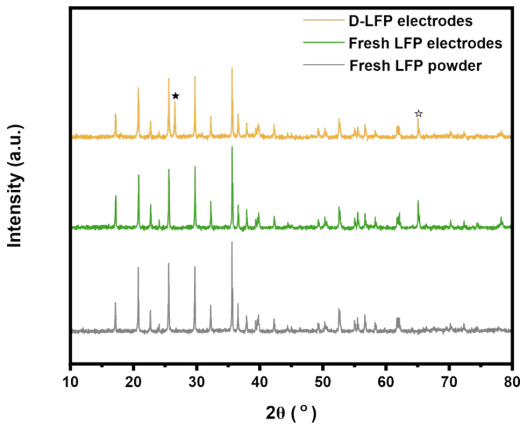

Fig. S24 XRD patterns of fresh LFP powder, fresh LFP electrodes, and D-LFP electrodes.

As shown in Figure S24, the diffraction peak around 26° labeled ★ is assigned to the (002) plane of conductive carbon, whereas the peak labeled ☆ at around 65° arises from the (220) reflection of the aluminum current collector.

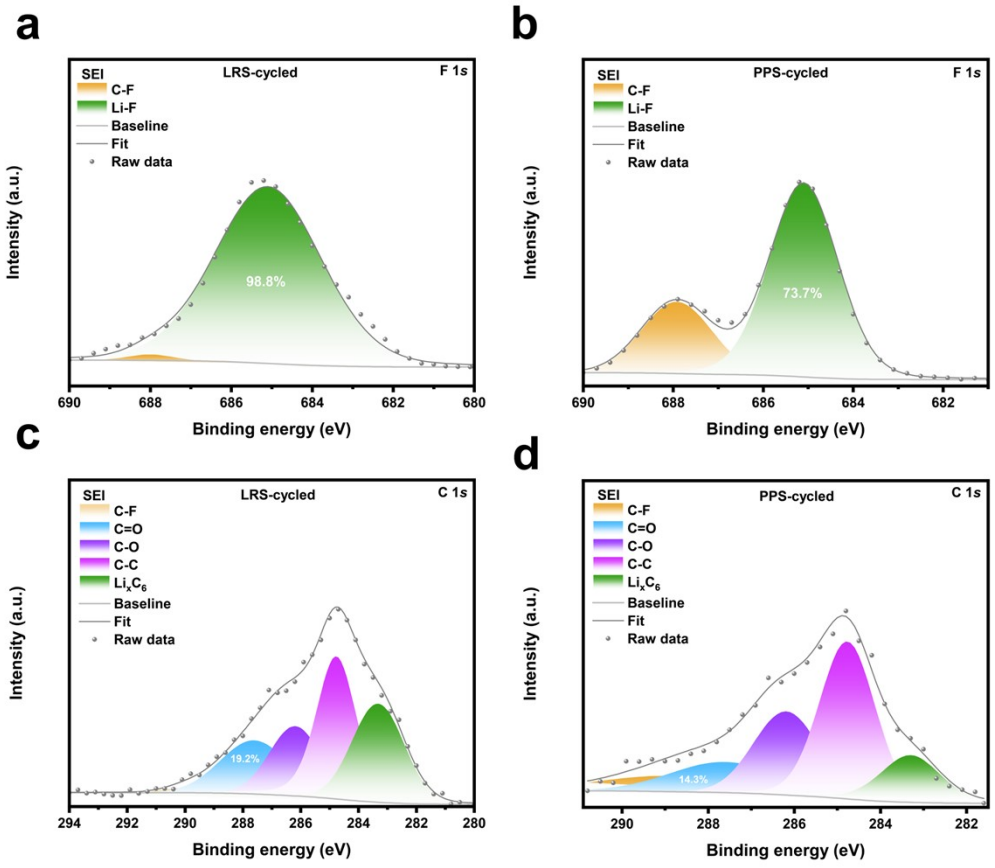

Fig. S25 XPS F 1s and C 1s spectra of the SEI for LRS-cycled cells (a, c) and PPS-cycled cells (b, d).

In the F 1s spectra (Figure S25a-b), the main peaks at ~685.1 and ~688 eV are assigned to Li-F and C-F species,[1-3] respectively. In the C 1s spectra (Figure S25c-d), the main peaks at ~283.3, 284.8, 286.2, 287.6, and 290.0 eV are attributed to Li_xC_6, C-C, C-O, C=O, and C-F species,[1, 3-6] respectively.

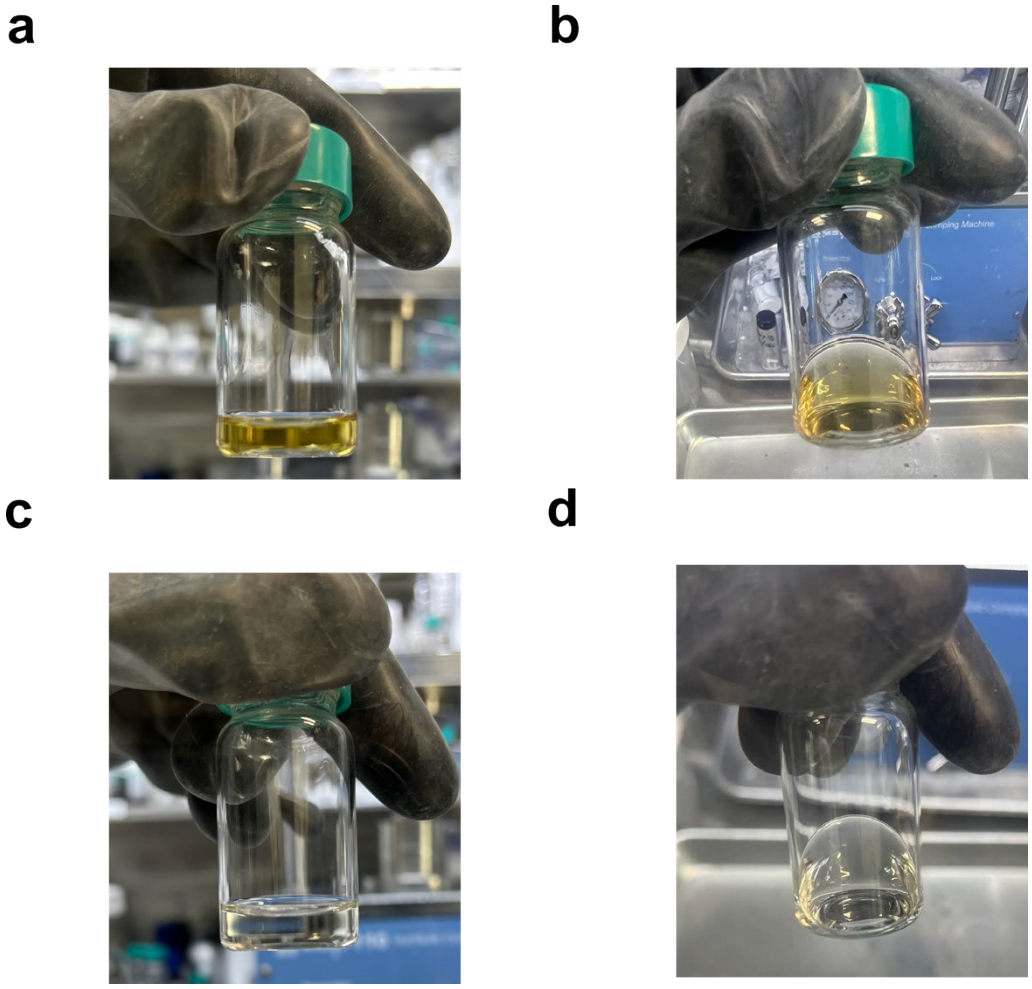

Fig. S26 Photos of (a-b) 0.1 M TFBQ-LP57 electrolyte and (c-d) LP57 at different viewing angles.

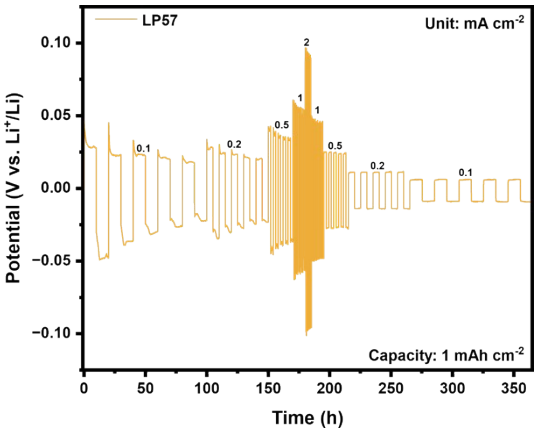

Fig. S27 Galvanostatic rate performance of LP57 symmetrical cells, at current densities of 0.1-2 mA cm^{-2}, with a fixed capacity of 1 mAh cm^{-2}.

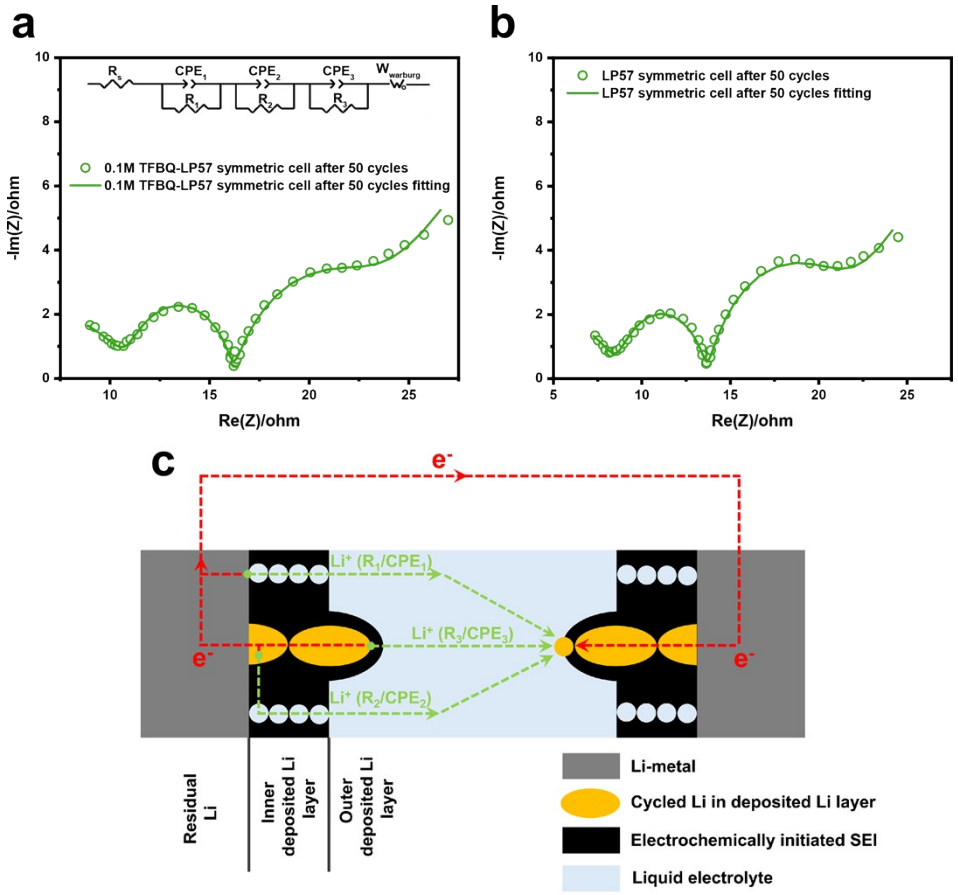

Fig. S28 Raw and fitted Nyquist plots of the impedance spectra of (a) 0.1 M TFBQ-LP57 and (b) LP57 symmetrical cells after the first 50 cycles. (c) Schematic illustration of the three interfacial structures and electrochemical process in the Li-Li symmetrical cell.

As shown in Figure S28, referring to the reported equivalent circuit[7] (inset of Figure S28a), the fitting results indicate that at least three interfacial structures (Figure S28c) coexist in the 0.1 M TFBQ-LP57 and LP57 symmetrical cells, originating from (I) residual Li | liquid electrolyte (R_1/CPE_1), (II) cycled Li in the inner deposited Li layer | liquid electrolyte (R_2/CPE_2), and (III) cycled Li on the outer deposited Li layer | liquid electrolyte (R_3/CPE_3). The 0.1 M TFBQ-LP57 cell exhibits an R_s of 1.6 Ω, with R_1 = 5.9 Ω, R_2 = 4.9 Ω and R_3 = 9.6 Ω with a $\chi^2/|Z|$ of 0.0027. These values are comparable to those of the LP57 cell, which has an R_s of 0.3 Ω, R_1 = 4.7 Ω, R_2 = 6.6 Ω and R_3 = 8.6 Ω with a $\chi^2/|Z|$ of 0.0032.

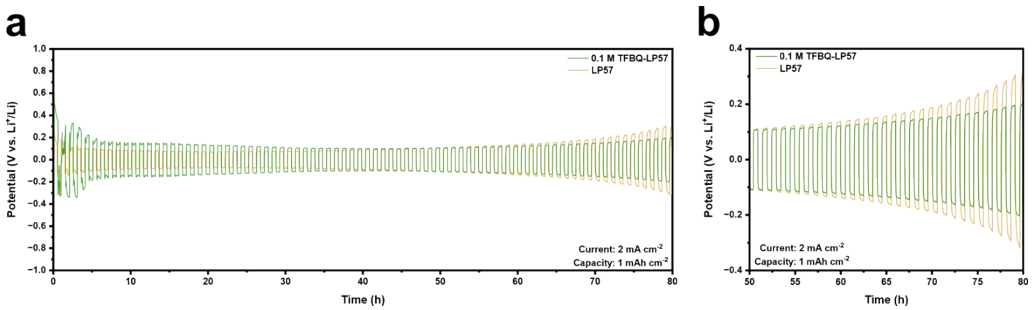

Fig. S29 Galvanostatic cycling performance of LP57 and 0.1 M TFBQ-LP57 symmetrical cells at 2 mA cm^{-2}/1 mAh cm^{-2} for (a) 80 h, with the zoomed-in region from (b) 50 to 80 h.

2. Supporting Tables

Table S1 Li content of the as-synthesized LTFBB.

Li purity in fresh LTFBB (%)	Theoretical atomic weight of Li in LTFBB (%)	Li content of as-synthesized LTFBB (%)
99.2	7.2	7.14

As shown in Table S1, the Li content in LTFBB is calculated by multiplying the Li purity of LTFBB, measured by ICP, by the theoretical Li atomic weight in LTFBB. The resulting Li content in fresh LTFBB (denoted $Li\ content\ in\ fresh\ LTFBB$) is:

$$Li\ content\ in\ fresh\ LTFBB = Li\ purity\ in\ fresh\ LTFBB \times Theoretical\ atomic\ weight\ of\ Li\ in\ LTFBB = 99.2\% \times 7.2\% = 7.14\%$$

Table S2 Theoretical atomic weight of LTFBB.

C	O	F	Li
37.1%	16.5%	39.2%	7.2%

Table S3 Li content of LTFBB after decomposition and the decomposition percentage of LTFBB during charging to 4.3 V.

Li purity in LTFBB after decomposition (%)	**Theoretical atomic weight of Li in LTFBB (%)**	**Li content of LTFBB after decomposition (%)**	**Decomposition percentage of LTFBB (%)**
43.4	7.2	3.12	56.3

Table S3 presents the Li content in LTFBB after decomposition, which is determined by multiplying the Li purity measured by ICP by the theoretical Li atomic weight of Li in LTFBB. The resulting Li content after decomposition (denoted $Li\ content\ after\ decomposition\ of\ LTFBB$) is:

$$\begin{aligned} &Li\ content\ after\ decomposition\ of\ LTFBB \\ &= Li\ purity\ in\ LTFBB\ after\ decomposition \times Theoretical\ atomic\ weight\ o \\ &= 43.4\% \times 7.2\% = 3.12\% \end{aligned}$$

Correspondingly, the decomposition percentage of LTFBB (denoted $Decomposition\ percentage\ of\ LTFBB$), as shown in Table S3, is:

$$\begin{aligned} &Decomposition\ percentage\ of\ LTFBB \\ &= \frac{The\ Li\ content\ of\ fresh\ LTFBB - The\ Li\ content\ of\ LTFBB\ after\ decom}{The\ Li\ content\ of\ fresh\ LTFBB} \\ &= \frac{7.14\% - 3.12\%}{7.14\%} = 56.3\% \end{aligned}$$

Table S4 Amount of TFBQ generated during LTFBB decomposition and the concentration of generated TFBQ in the electrolyte.

Areal loading of LTFBB on LRS (mg cm^{-2})	**Generated TFBQ amount (mg cm^{-2})**	**Concentration of generated TFBQ in the electrolyte (mM)**
~0.15	~0.0467	~7.46
~0.3	~0.0935	~14.9
~0.4	~0.1249	~19.9
~0.65	~0.2055	~32.7
~1	~0.3145	~50.1

As shown in Table S3, the decomposition percentage of LTFBB is approximately 56.3%. Therefore, for LRS with different LTFBB loadings of ~0.15, 0.3, 0.4, 0.65, and 1 mg cm^{-2}, the generated TFBQ is about 0.0467, 0.0935, 0.1249, 0.2055, and 0.3145 mg cm^{-2}, respectively. The corresponding concentration of TFBQ in the electrolyte is approximately 7.46, 14.9, 19.9, 32.7, and 50.1 mM.

Supporting References

1. Z. Zhang, J. Hu, Y. Hu, H. Wang and H. Hu, *Ionics*, 2024, **30**, 3951-3961.
2. W. Wu, A. Wang, Q. Zhan, Z. Hu, W. Tang, L. Zhang and J. Luo, *Small*, 2023, **19**, 2301737.
3. R. Azmi, F. Lindgren, K. Stokes-Rodriguez, M. Buga, C. Ungureanu, T. Gouveia, I. Christensen, S. Pal, A. Vlad, A. Ladam, K. Edström and M. Hahlin, *ACS Appl. Mater. Interfaces*, 2024, **16**, 34266-34280.
4. V. Sharova, A. Moretti, T. Diemant, A. Varzi, R. J. Behm and S. Passerini, *J. Power Sources*, 2018, **375**, 43-52.
5. M. Lu, H. Cheng and Y. Yang, *Electrochim. Acta*, 2008, **53**, 3539-3546.
6. G. M. Veith, M. Doucet, R. L. Sacci, B. Vacaliuc, J. K. Baldwin and J. F. Browning, *Scientific Reports*, 2017, **7**, 6326.
7. J.-J. Woo, V. A. Maroni, G. Liu, J. T. Vaughey, D. J. Gosztola, K. Amine and Z. Zhang, *J. Electrochem. Soc.*, 2014, **161**, A827.